Climate Dynamics (2021) 56:245–257
https://doi.org/10.1007/s00382-020-05480-3

The role of internal variability in multi-decadal trends of summer rainfall over East Asia–Northwest Pacific

Ruyu Gan[1,3] · Kaiming Hu[1] · Gang Huang[1,2,3]

Received: 27 May 2020 / Accepted: 2 October 2020 / Published online: 10 October 2020

Abstract

The impacts of internal variability on East Asia–Northwest Pacific (EA–NWP) summer rainfall trends on the multidecadal time scale are invested based on three large ensemble simulations, which have ensemble member of 30, 40 and 100. In all the three simulations, the summer rainfall trends during 1970–2005 are remarkably diverse across the individual ensemble members over the EA–NWP, and the signal-to-noise ratio is lower than 1 over the EA–NWP, suggesting a strong impact of internal variability on EA–NWP summer rainfall trends at this interval. Moreover, we found that the diversity of EA–NWP summer rainfall trends across individual members has a similar leading spatial pattern in all the three ensembles, featuring reverse trends between in Mei-yu region and in the tropical NWP. The leading pattern is likely caused by a gradient between the sea surface temperature (SST) trends in the North Indian Ocean (NIO) and in the tropical western Pacific (WP). When there is a warming trend in the NIO and a cooling trend in the tropical WP, a low-level anomalous anticyclone strengthens over the subtropical NWP, causing a dipole rainfall trend over the EA–NWP. The impact of the east–west SST gradient pattern is confirmed by numerical experiments. Our findings highlight that the internally-generated gradient of NIO–WP SST trends is an important source of the uncertainty in EA–NWP summer rainfall decadal changes in simulations.

Keywords East Asia summer rainfall · Internal variability · Anomalous anticyclone

1 Introduction

In the monsoon region of East Asia, where more than 100 million people live, the summer rainfall has experienced a prominent change in recent decades. In China, the change of rainfall since the late 1970s mainly features a south-flood-north-drought (SFND) pattern, characterized by an increase of rainfall in the south and a decrease of rainfall in the north (Hu 1997; Xu 2001). The rainfall changes have caused severe droughts in North China and frequent flooding along the Yangtze River and South China during recent decades, causing large losses in human lives and enormous damages to local economies (Huang et al. 2007). Meantime, prominent rainfall changes also have been found in the other East Asian regions such as southwest Japan and Korea (Wang et al. 2006). The rainfall changes in East Asia are associated with large-scale atmospheric circulation modulation, including a weakening of East Asian summer monsoon (Wang 2001; Yu et al. 2004), a southward shift of the 200 hPa jet stream (Yu et al. 2004; Yu and Zhou 2007; Schiemann et al. 2009), and an intensification and a westward extension of western Pacific subtropical high (Hu 1997; Gong and Ho 2002). Generally, two main lines of reasons have been proposed to explain the multi-decadal changes of summer rainfall in East Asia.

One is to attribute the rainfall changes to the effect of anthropogenic forcing, including changes in aerosol emission and greenhouse gas concentration (Menon et al. 2002; Zhou et al. 2009a). Numerical model simulations show that

✉ Kaiming Hu
hkm@mail.iap.ac.cn

✉ Gang Huang
hg@mail.iap.ac.c

1 State Key Laboratory of Numerical Modeling for Atmospheric Sciences and Geophysical Fluid Dynamics and Center for Monsoon System Research, Institute of Atmospheric Physics, Chinese Academy of Sciences, P.O. Box 9804, Beijing 100029, China

2 Laboratory for Regional Oceanography and Numerical Modeling, Qingdao National Laboratory for Marine Science and Technology, Qingdao 266237, China

3 University of Chinese Academy of Sciences, Beijing 100049, China

the increasing of aerosol emission in East Asia could cool the Asian continent and weaken land–ocean thermal contrast between Asian continent and the NWP (Wang et al. 2013b; Song et al. 2014; Dong et al. 2015). Consequently, the monsoon circulation turns weak and brings less vapor to North China, causing a drying trend over North China (Ohba and Ueda 2006; Wang et al. 2015). Unlike the dynamic effect of aerosol forcing, the increase of greenhouse gas concentration affects East Asian summer rainfall mainly via thermodynamic processes (He et al. 2012; Li et al. 2015). The greenhouse gas-induced global warming makes atmospheres more humid, which in turn results in increasing precipitation in monsoon rainfall belt, obeying the so-called wet-get-wetter process (Chou and Neelin 2004; Held and Soden 2006; Chou et al. 2009; He et al. 2012). Moreover, some processes related to the land-sea temperature contrast and the relative humidity are also important for the monsoon rainfall changes over the land, which complements the "wet-get-wetter" process for the thermodynamic processes (Byrne and O'Gorman 2013; Byrne and O'Gorman 2015). Model experiments show that the combined effects of increases in greenhouse gases and aerosol emissions help to weaken East Asian summer monsoon circulation (Song et al. 2014; He et al. 2019) and form the SFND rainfall trend since the early 1970s (Wang et al. 2013b; Tian et al. 2018).

The other is to attribute to the internally generated low-frequency variability in climate system. Using a 123-year precipitation data (1880–2002) at 35 stations in East China, Ding et al. (2008) revealed that the variations of summer rainfall in China has a considerable component of interdecadal oscillation, with the period varying from 12 to 80-year. For example, in North China, significant above-normal precipitation occurred from 1940s to the 1970s, while below-normal precipitation was observed from the 1890s to the 1930s and from 1980s to the 1990s. The multidecadal oscillations in rainfall in turn are likely linked to the multi-decadal variations of the tropical sea surface temperature, especially the Pacific decadal oscillation (PDO) (Ma 2007; Zhou et al. 2009a; Qian and Zhou 2014; Song and Zhou 2015; Ueda et al. 2015; Zhang and Zhou 2015). In the positive PDO phase, atmospheric circulation anomalies over the EA–NWP regions feature an anomalous Pacific-Japan (Nitta 1987)/East Asian-Pacific (Huang and Wu 1989) (PJ/EAP) teleconnection-like pattern in response to Tropical Indian Ocean (TIO) warming, with a high-pressure system over the North China reducing rainfall in North China, and vice versa (Qian and Zhou 2014). Beside the PDO, the multi-decadal changes of SST in the central and the eastern Pacific (Li et al. 2010; Wang et al. 2013a; Xiang et al. 2013; He and Zhou 2015; Li et al. 2019) and the Indian Ocean (Yang et al. 2007; Li et al. 2008; Xie et al. 2009, 2016; Kosaka et al. 2013) are also considered to affect summer precipitation over East Asia through influencing on the subtropical northwestern Pacific high (SNPH). Furthermore, Wu et al. (2019) recently found that the SFND-like pattern of multi-decadal rainfall change can result from atmospheric internal variability.

Thus, both external forcing and internal variability likely contribute to the multi-decadal trends of summer rainfall in East Asia. However, the relative contribution of each has not yet been known. It is often difficult to distinguish the internally-generated low-frequency variability and externally-forced climate change by analyzing observations. Deser et al. (2012a) and Wallace et al. (2012) developed a methodology to separate the forced climate change and internally generated variability using a large ensemble of simulation with a single climate model. Each ensemble member starts from a randomly perturbed initial atmospheric condition and is subject to the same prescribed time-varying radiative forcing. This follows from the fact that one given climate model contains both intrinsic and external forced climate changes. The ensemble-mean trends provide an estimated of the forced response of the model and the resulting difference in behavior of the ensemble members can be identified as the internal variability of the climate model. Many previous studies have examined the intrinsic and externally forced contribution in climate trends with such an initial-condition large ensemble conducted with a fully-coupled global model (Deser et al. 2012a, b; Wallace et al. 2012; Hu et al. 2018). The method is proved to be effective to separate the role of the forced climate change and internal variability.

Here, to avoid model dependence, we use three large ensembles: (1) a 30-member ensemble of simulations of Version 4 of the Community Climate System Model (CCSM4) (Gent et al. 2011), (2) a 40-member ensemble of simulations by the CESM Large Ensemble project (Kay et al. 2015) and (3) a 100-member ensemble of simulations by the Max Planck Institute Earth System Model (MPI-ESM) (Maher et al. 2019). In this study, we aim to answer the following questions: (1) What are the relative contribution of external forcing and internal variability to the recent multi-decadal trends of summer rainfall in East Asia? (2) How does the internal variability affect multi-decadal trends of summer rainfall in East Asia?

The remainder of the paper is organized as follows. Section 2 provides a description of the data and methods used in this study. Section 3 shows the relative contribution of internally-generated variability and externally-forced climate change to East Asian summer rainfall trends. Section 4 demonstrates the leading modes of internally-generated rainfall trends over East Asian and their corresponding atmosphere circulation, SST and wave activity flux anomalies. Section 5 presents the role of NIO-WP SST gradient. Section 6 gives the summary.

2 Data and method

2.1 Model simulations

Following Deser et al. (2012a), we first used 30-member ensemble simulations to evaluate the role of internal variability in multidecadal trends of East Asian summer rainfall. The ensemble simulations are conducted by Version 4 of the Community Climate System Model (CCSM4) for the period 1970–2005 (https://www.earthsystemgrid.org). CCSM4 is a comprehensive coupled atmosphere–ocean–sea ice-land general circulation model at a horizontal resolution of approximately 0.94 latitude and 1.25 longitude. Each ensemble member undergoes the same external forcing that is the same as that using in the phase 5 of the Coupled Model Intercomparion Project (CMIP5). Each member begins from identical initial conditions in the ocean, land, and sea ice model components but slightly different initial conditions in the atmospheric model. More details of the model's formulation and performance can be found in Gent et al. (2011).

We also use a 40-member ensemble simulation by the CESM Large Ensemble project (Kay et al. 2015) and a 100-member Grand Ensemble generated by the MPI-ESM (Maher et al. 2019) to examine whether internal variability generally exists in other climate models. The CESM Large Ensemble make use of the fully coupled CESM, version 1 with the Community Atmosphere Model, version 5 (CESM1-CAM5) (Hurrell et al. 2013) at approximately 18 horizontal resolution in the ocean and atmosphere. Each ensemble member is forced with the CMIP5 historical forcing in the period 1920–2005 (https://www.earthsystemgrid.org). The MPI-ESM has a T63L47 configuration in the atmosphere and 40 vertical levels in the ocean. The historical simulations of the MPI-ESM ensemble begin in 1850 and are forced with the CMIP5 historical forcing until 2005 (https://esgf-data.dkrz.de/search/mpi-ge/).

2.2 Observational data

The Chinese daily rainfall data comprising 824 surface stations are derived from the Chinese Meteorological Data Center, China Meteorological Administration from 1970 to 2005 (http://data.cma.cn/data). Stations were excluded when there were one or more days of missing data; Thus, 725 stations were selected to ensure data consistency over the study period.

2.3 Method

We analyze the period 1970–2005 from each ensemble member and compute linear trends over this 36-year period for summer (June–July–August). Performing the empirical orthogonal function (EOF) analysis on the departures of the precipitation trends from the ensemble mean to extract the leading patterns of internal variability-induced precipitation trends in EA–NWP. For each large ensemble, the external forcing is the same for the all the individual members, and the difference among the individual members should be due to internal variability. Therefore, the leading EOF modes could be considered as the major patterns of internal variability-induced precipitation trends in EA–NWP. The SST and circulation anomalies associated with the precipitation EOF modes are calculated by regression on the corresponding principal components (PCs). We use the Student's t-test to test the significance of long-term trends for the spatial patterns based on valid freedom. In this paper, the term "trend" denotes the linear trend.

3 Internal and external parts of total trends

During the period from 1970 to 2005, the observed summer rainfall in China stations experienced a significant change. Wetting trends are mainly distributed in the southeast of China, with the maximum wetting rate over 2 mm day^{-1} 36^{-1} year^{-1}, while observed drying trends mainly exists in the North China. The observed rainfall trends generally feature a dipole pattern in China. Figures 1 and 2 examine the summer precipitation trends over 1970–2005 from each run of CESM and CCSM4, respectively. Although each simulation shares the same external forcing in the same model, summer precipitation trends display considerable member-to-member diversity in EA–NWP. Specifically, some ensemble members (runs #5, #25 and #30) in CESM and some ensemble members (runs #8, #21 and #25) in CCSM4 exhibit positive–negative meridional structure over EA–NWP which are similar to the observed rainfall trend pattern, while some other members (runs #10 and #15) in CESM and (runs #4, #5 and #14) in CCSM4 show reverse structure in EA–NWP. The summer precipitation trends over 1970–2005 in the 100-member ensemble of MPI-ESM simulations also show strong member-to-member diversity (figure not shown). In each ensemble, all the individual members are forced by the same external forcing in the same model, the large diversity across the individual ensemble members suggests the important role of internal variability in summer rainfall trend in EA–NWP on the multidecadal time scale.

Figure 3a, d, g show the ensemble-mean JJA precipitation trends over 1970–2005 in CCSM4, CESM and MPI-ESM ensemble simulations, respectively. Despite some differences among the three models, the ensemble-mean JJA precipitation trends in all the three ensembles display a dipole structure over the EA–NWP, with positive rainfall trends in the subtropical NWP but negative rainfall trend to the north,

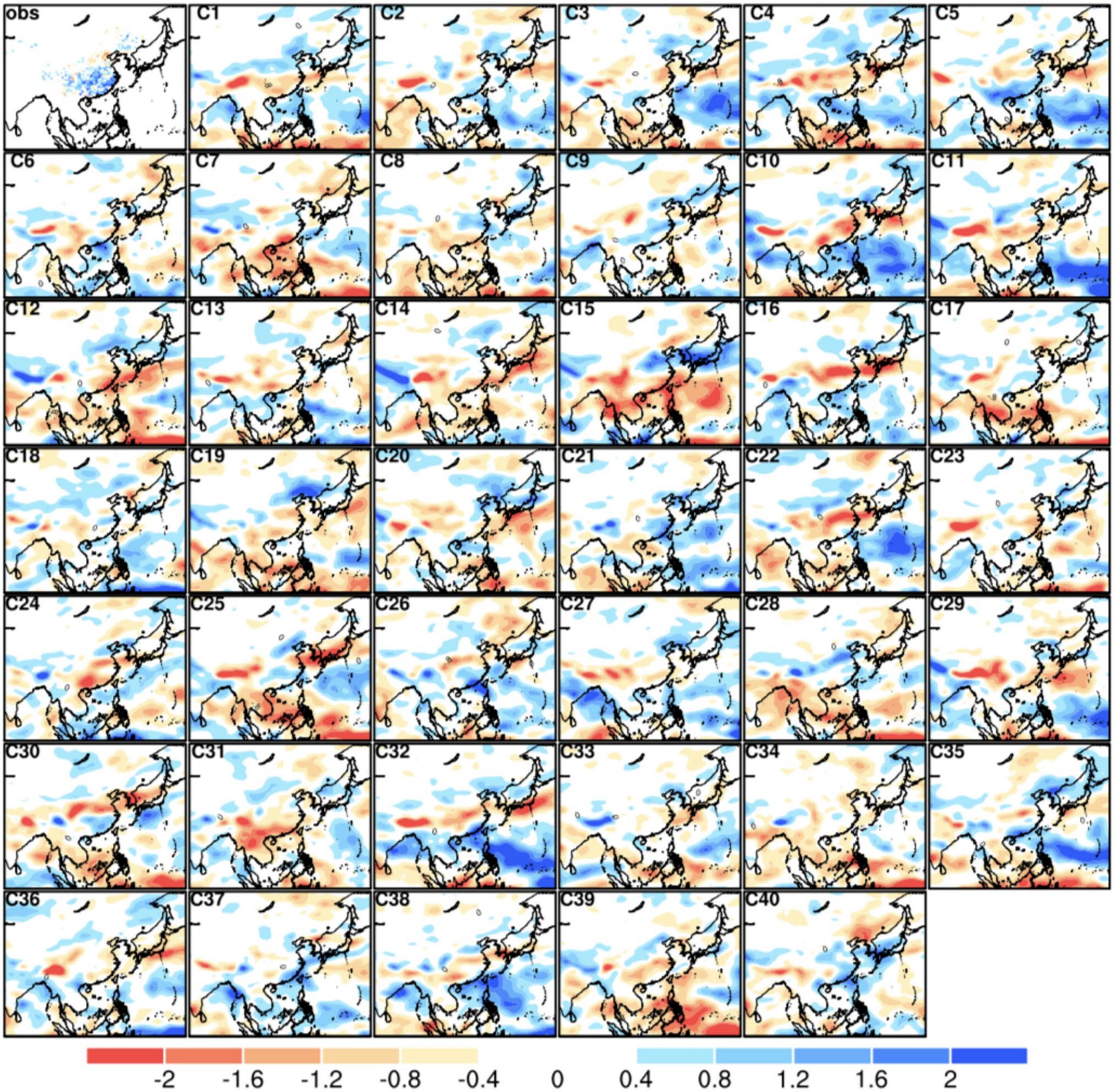

Fig. 1 JJA rainfall trends (1970–2005; mm day^{-1} 36^{-1} year^{-1}) in observation and in each of the 40 CESM ensemble members

indicating that external forcing could lead to the south-north opposite rainfall trends over the EA–NWP. Compared with the observations, the ensemble-mean precipitation trend in CCSM4 (Fig. 3a) is similar in shape but much smaller in magnitude, consistent with the model study by He et al. (2012), suggesting that the observed rainfall trends should be only partly contributed by external forcing.

In order to quantify the relative contribution of internally-generated low-frequency variability and externally-forced changes in JJA precipitation trends (1970–2005), we used the signal-to-noise ratio of the ensemble mean precipitation trends to the standard deviation of the departures. For CCSM ensemble simulations, the standard deviation of the JJA precipitation trends is shown in Fig. 3b, which is larger than 1.2 mm day^{-1} 36^{-1} year^{-1} in the latitudinal band of 10° N–30° N and smaller than 0.9 mm day^{-1} 36^{-1} year^{-1} in the high latitudes. The signal-to-noise ratio between the ensemble-mean JJA precipitation trends and the standard deviation are less than 1.0 in nearly all of the region over EA–NWP. In the Yangtze river valley and the regions around Lake Baikal, the ratio is small than 0.2. The ratio ranges from 0.4 to 0.6 in the subtropical NWP,

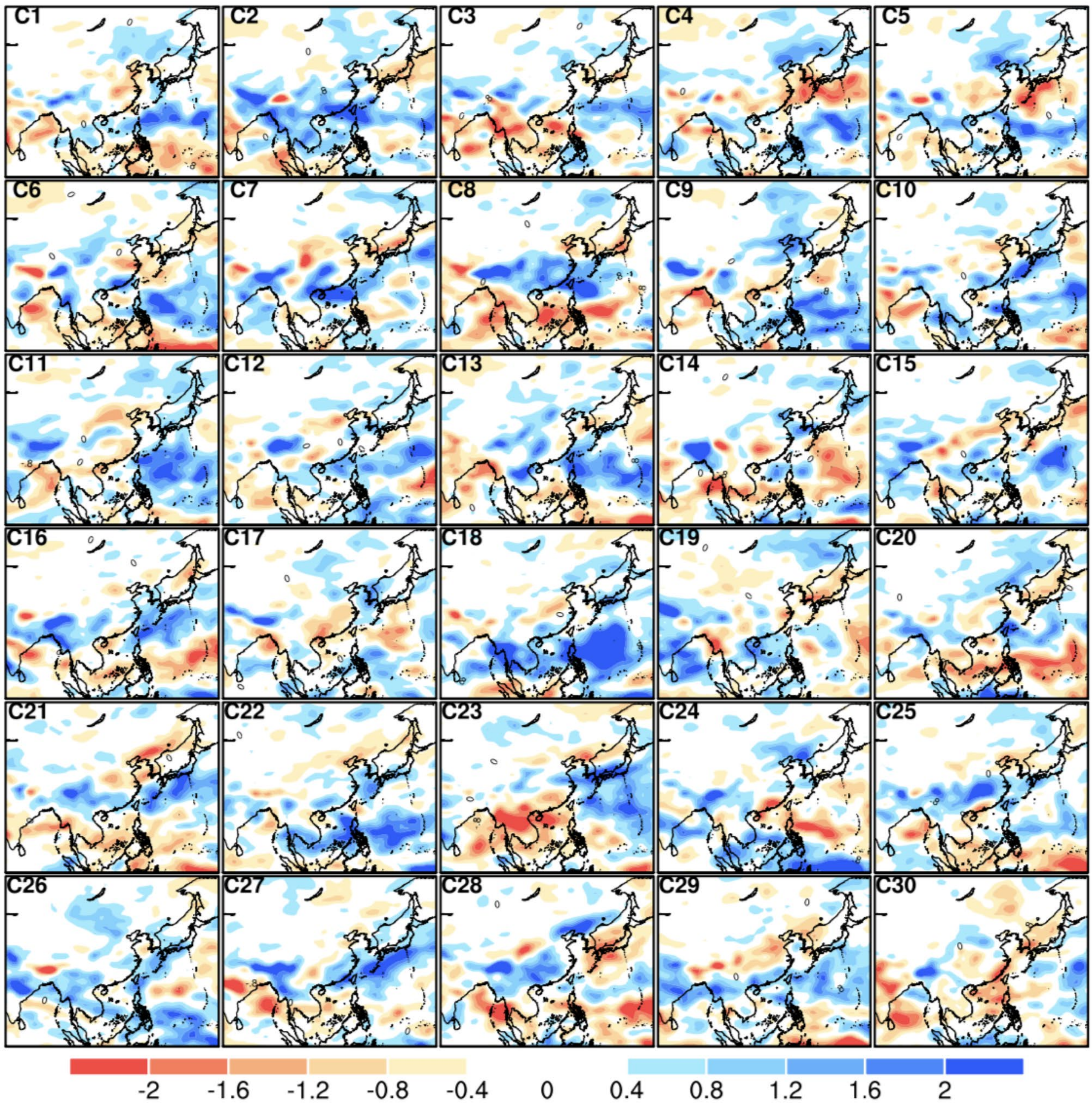

Fig. 2 JJA rainfall trends (1970–2005; mm day^{-1} 36^{-1} year^{-1}) from each of the 30 CCSM4 ensemble members

Southwest China and North China. Similar results also exist in the CESM (Fig. 3e, f) and the MPI (Fig. 3h, i) ensemble simulations. Although there are some differences in the ensemble-mean JJA precipitation trends among the three models, all the three ensemble simulations show that the summer rainfall changes in EA–NWP display a large diversity among individual members, indicating a profound influence of internal variability to multidecadal summertime precipitation change over EA–NWP.

4 Leading mode of internal variability

The summer EA–NWP precipitation trends show a notable diversity among the individual members in all the three simulations. In order to find out the coherent spatial pattern of internally generated precipitation trends, we perform an EOF analysis of ensemble precipitation trends in the domain of EA–NWP (10°–50° N, 90°–140° E) among

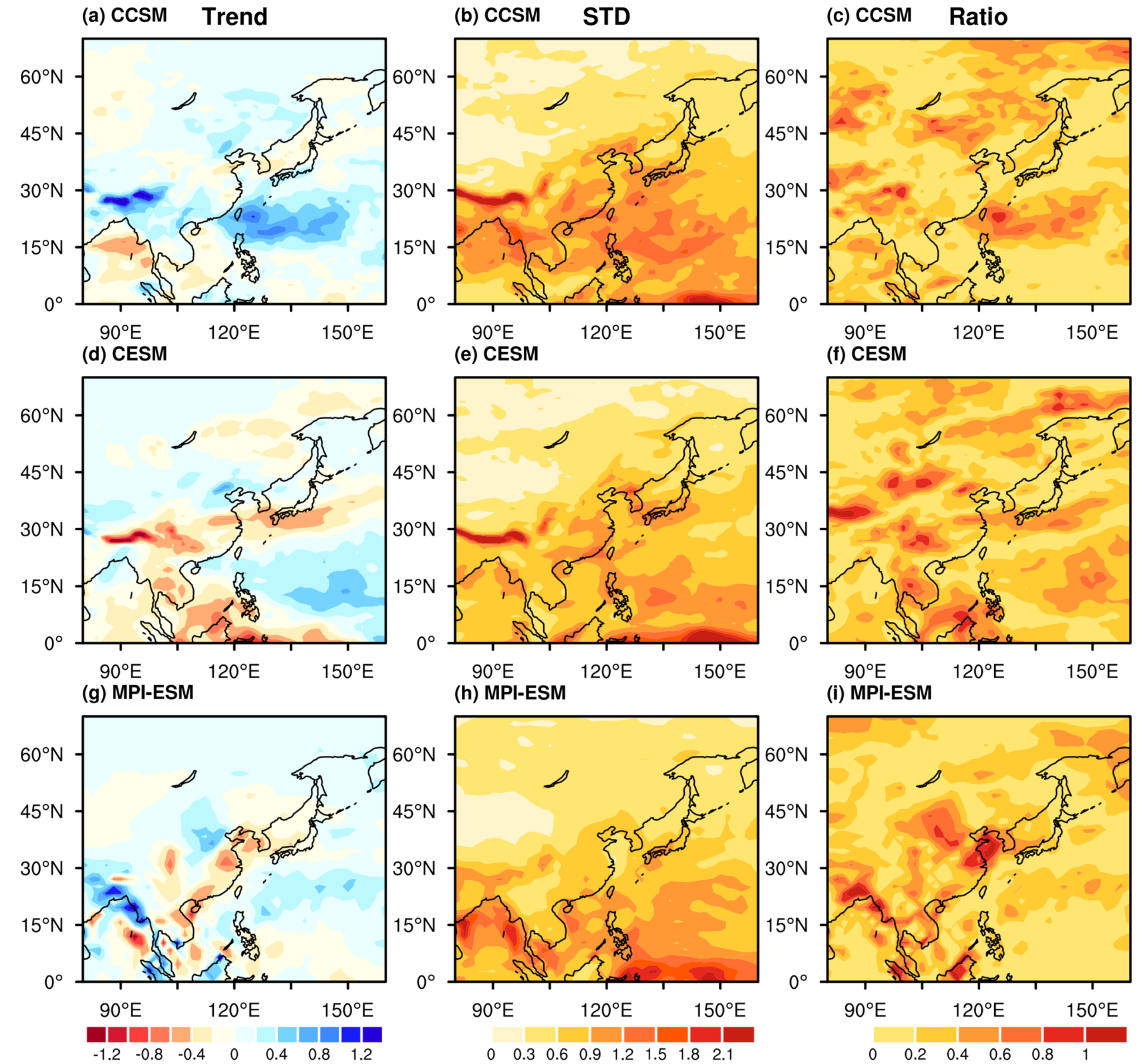

Fig. 3 The ensemble-mean rainfall trends during 1970–2005 (mm day^{-1} 36^{-1} year^{-1}) in CCSM4 (**a**), the standard deviation of the rainfall trends (**b**), and the ratio of the ensemble mean to the standard deviation of rainfall trends among the 30 CCSM4 ensemble members (**c**). **d**–**f** In CESM and **g**–**i** in MPI-ESM

all ensemble members for CCSM4, CESM and MPI-ESM simulations, respectively.

The EOF1s are well separated from the others according to the criterion of North (North et al. 1982) and account 19.7%, 24.4% and 14.7% for CCSM, CESM and MPI-ESM, respectively. Figure 4a–c show the regression maps of precipitation trends upon the first leading principle components (PC1s) for CCSM, CESM and MPI-ESM, respectively. In all the three models, the EOF1 modes feature a meridional dipole in precipitation trends, with positive values in the Mei-yu Front rainfall belt (20°–35° N) and negative values in the tropical NWP. It is interesting to notice that the spatial structures of the leading internal model are similar to those in the ensemble-mean rainfall trends. The results suggest that the observed summer rainfall trends over the EA–WNP are likely affected by both internal variability and external forcing.

How does the leading internal variability pattern generate? Figure 5a, b show the upper and the lower tropospheric atmospheric circulation associated with the EOF1 mode in CCSM4. Associated with the dipole pattern in rainfall trends, there is a prominent anomalous anticyclone over the

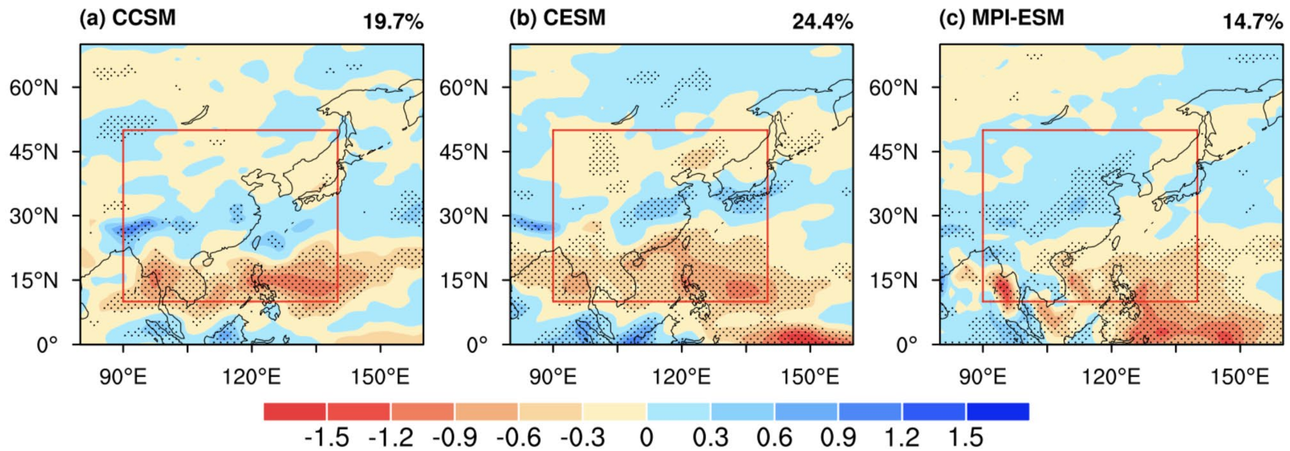

Fig. 4 Regressions of summer rainfall trends (1970–2005; shading; mm day^{-1} 36^{-1} year^{-1}) among the ensemble members upon the normalized PC1 of EOF modes of rainfall trends in the domain of East Asia–Northwest Pacific (10°–50° N, 90°–140° E) in **a** CCSM4, **b** CESM and **c** MPI respectively. The dots represent passing the 95% confidence level

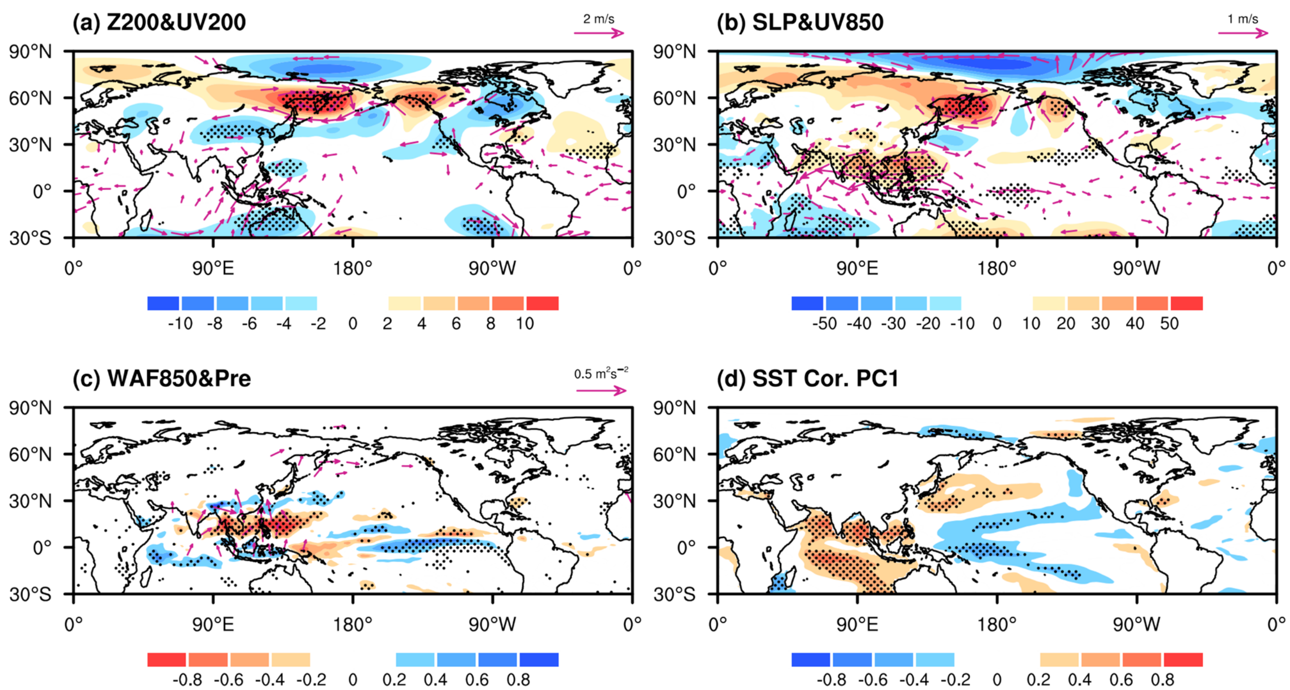

Fig. 5 Regression of JJA geopotential height trends (Pa 36^{-1} year^{-1}; shading) and winds trends (m s^{-1} 36^{-1} year^{-1}; vectors) at 200 hPa (**a**) and SLP trends (Pa 36^{-1} year^{-1}; shading) and winds trends (m s^{-1} 36^{-1} year^{-1}; vectors) at 850 hPa (**b**) on the normalized PC1 in CCSM. The wave activity flux at 850 hPa (m^2 s^{-2} 36^{-1} year^{-1}; vectors) and rainfall trends (shading) associated with the EOF1 mode with the PC1 in CCSM4 (**c**). Correlations of JJA SST trends with the PC1 in CCSM4 (**d**). The dots represent passing the 95% confidence level

tropical NWP at 850 hPa. At 200 hPa, there are the cyclonic anomalies over the tropical NWP, indicating that the circulation anomalies are baroclinic there. For CESM (Fig. 6a, b) and MPI-ESM (Fig. 7a, b), the anticyclonic center and cyclonic center over the tropical NWP are also significant in the lower and the upper level, respectively. The atmospheric circulation anomalies are dynamically consistent with the dipole rainfall trend. On one hand, the anomalous anticyclone over the tropical NWP can decrease local rainfall but increase East Asian summer monsoon rainfall, thus leading to the meridional dipole rainfall belt over the regions of EA–NWP (Wang et al. 2003). On the other hand, the rainfall

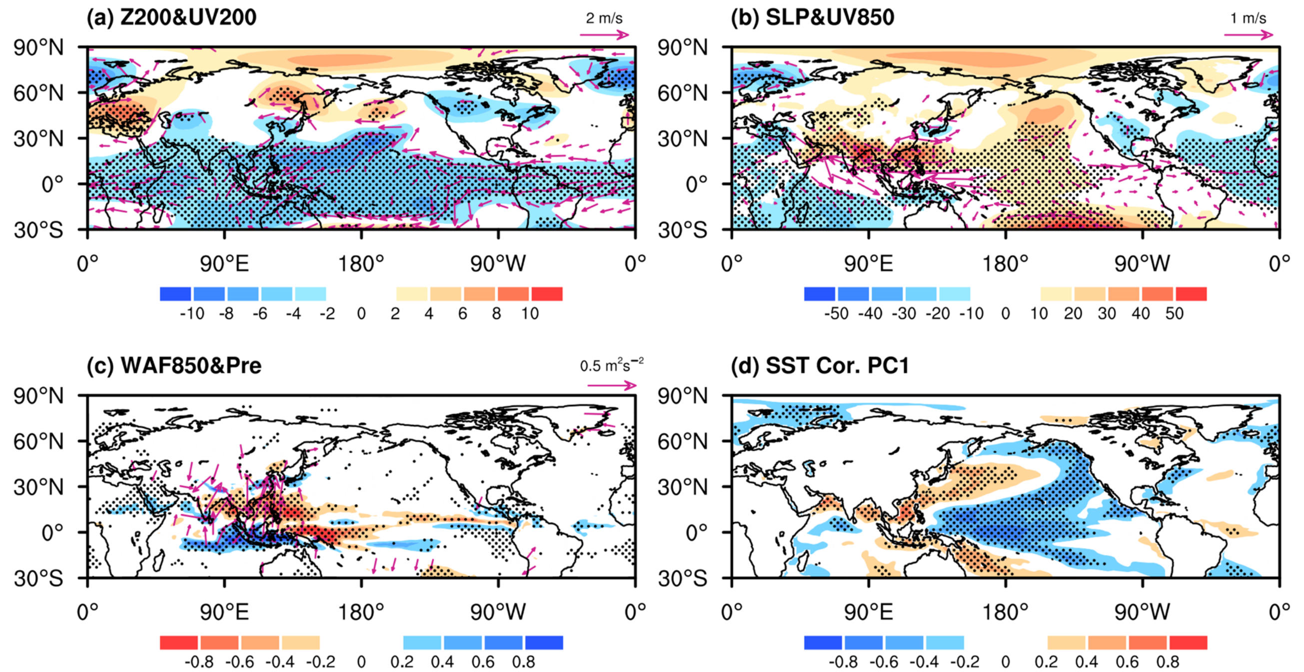

Fig. 6 As in Fig. 5 but for the CESM

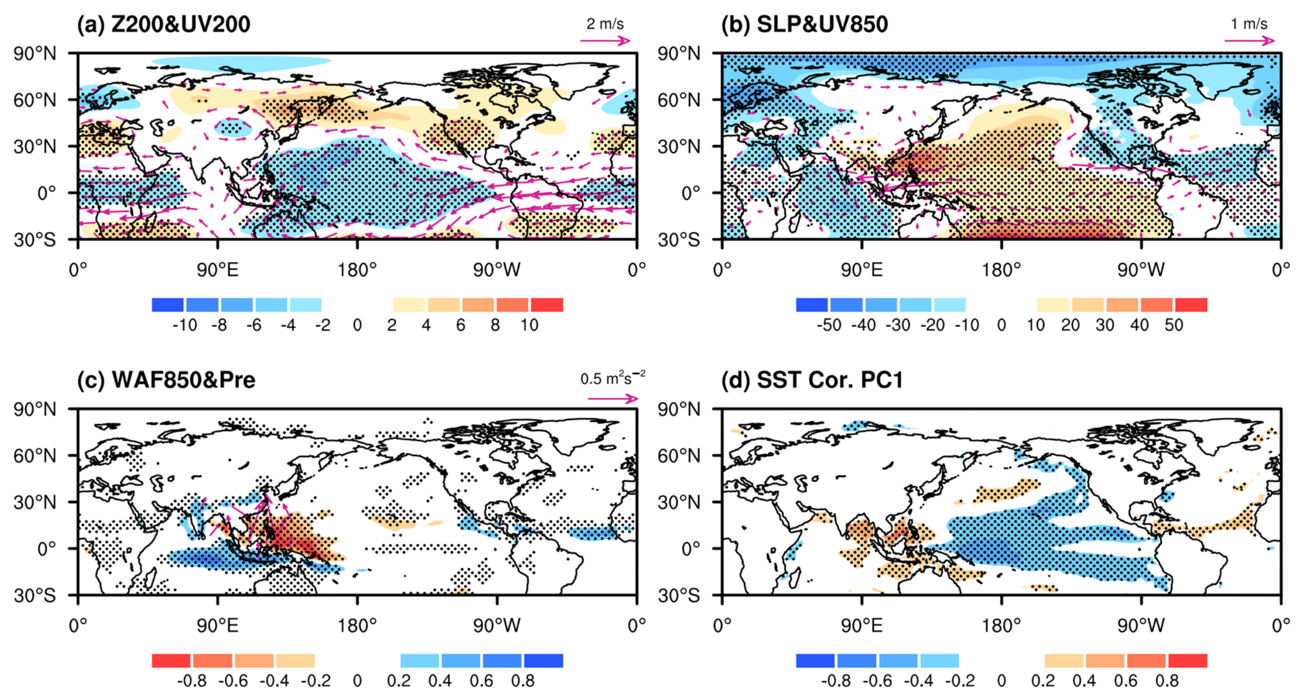

Fig. 7 As in Fig. 5 but for the MPI-ESM

anomaly can induce the atmospheric circulation anomalies via exciting baroclinic Rossby wave. The result suggests that the leading mode of internally-generated precipitation trends over the EA–NWP is linked to the anomalous anticyclone over the tropical NWP.

Figures 5c, 6c and 7c show the wave-activity fluxes associated with the EOF1 mode in CCSM, CESM, and MPI-ESM simulations, respectively. The definition of the wave-activity fluxes follows Takaya and Nakamura (2001) as:

$$W = \frac{1}{2|\mathbf{U}|}\begin{pmatrix} \bar{u}\left(\psi_x'^2 - \psi'\psi_{xx}'\right) + \bar{v}\left(\psi_x'\psi_y' - \psi'\psi_{xy}'\right) \\ \bar{u}\left(\psi_x'\psi_y' - \psi'\psi_{xy}'\right) + \bar{v}\left(\psi_y'^2 - \psi'\psi_{yy}'\right) \\ \frac{f^2}{R\sigma/p}\left\{\bar{u}\left(\psi_x'\psi_p' - \psi'\psi_{xp}'\right) + \bar{v}\left(\psi_y'\psi_p' - \psi'\psi_{yp}'\right)\right\} \end{pmatrix}. \quad (1)$$

Here, ψ denotes the stream function, f the Coriolis parameter, R the gas constant, $\mathbf{U} = (u, v)$ the horizontal wind velocity, and $\sigma = \left(R\bar{T}/C_p p\right) - d\bar{T}/dp$, with temperature T, and the specific heat at constant pressure C_p. Overbars and primes denote the climatology in JJA and the anomalies regressed on normalized PC1, respectively. The fluxes are parallel to the local group velocity of stationary Rossby wave. In all three models, there are notable northward wave activity fluxes from the tropical WP to East Asia, which could enhance rainfall in the Mei-yu Front rainfall belt (Huang and Sun 1992). The wave fluxes even propagate into Alaska via a great cycle path in CCSM and CESM models, in consistent with the wave-like geopotential height anomalies from the tropical NWP to high latitudes (Figs. 5, 6, 7b). These results indicate that the circulation and rainfall anomalies associated with the PC1 mainly arise from the tropics.

Figures 5d, 6d and 7d show the correlation of SST trend over 1970–2005 with the PC1 in CCSM, CESM and MPI-ESM, respectively. For CCSM simulations, there are significant positive correlations over the TIO and the subtropical Northwest Pacific (SNWP) but prominent negative correlations over the tropical western and central Pacific. For CESM (Fig. 6d), the positive values are over the North Indian Ocean and SNWP and negative values over the tropical western and central Pacific and Southern Indian Ocean (SIO). For MPI-ESM (Fig. 7d), there are also significant positive correlations in the NIO and negative correlations in tropical western and central Pacific. Although there are some differences in the SST pattern among the three models, they all show the east–west contrasting SST anomalies between the NIO and the tropical Pacific. Many previous studies have shown that such variability in the SST gradient between NIO and tropical Pacific contribute to the ACC over the NWP (Terao 2005; Chen et al. 2012; Cao et al. 2013; Xiang et al. 2013; Xie et al. 2016; Hu et al. 2019). The east–west contrasting SST anomalies between the NIO and the tropical Pacific weaken the walker circulation with significant easterly anomalies at 850-hPa (Figs. 5, 6, 7a) but westerly anomalies at 200-hPa over the tropical Indo-western Pacific (Figs. 5, 6, 7b) and suppress convection over the tropical western Pacific (Figs. 5, 6, 7c). The suppressed convection over the tropical western Pacific could form a low-level anticyclone residing to the northwest of the suppressed convection through exciting a Rossby wave response, which occurs with suppressed rainfall on its southeastern flank and enhanced rainfall in the Mei-yu Front rainfall belt (Wang et al. 2013a). Therefore, the EOF1 of precipitation trends is likely due to the internally-generated east–west contrasting SST variation between the NIO and the western and central Pacific on multidecadal time scale. The result is consistent with the observed result that the westward extension of WPSH since the late 1970s is likely caused by the warming trend in the NIO and cooling trend in WP (Hu 1997; Gong and Ho 2002; Zhou et al. 2009b).

5 Role of Indo-WP SST gradient

To further verify the role of the SST gradient between the NIO and the western and central Pacific, we conduct four experiments using the ECHAM5, which is an effective tool to study the atmospheric response to the SST anomalies (Xie et al. 2016; Jiang et al. 2019). A detailed description of ECHAM5 is given in Roeckner et al. (2003). The first experiment is forced by climatological SST and sea ice with a seasonal cycle, which is referred as control run. The second experiment, named as Run_NIO-WP_0.5, with the 0.5 °C SST anomalies in the NIO (0° N–20° N, 40° E–120° E) and − 0.5 °C SST anomalies in the WP (− 15° S–15° N,140° E–180° E) to be added in the climatological SST as the boundary conditions. The third (Run_NIO-WP_1.0) and the fourth experiments (Run_NIO-WP_1.5) are similar to the second experiment except for that the magnitudes of 1.0 °C and 1.5 °C SST anomalies are added, respectively. The last three experiments are referred as the sensitive runs. The details of SST boundary conditions in these experiments are given in in Table 1 and shown in Fig. 8a–c. Each experiment is run for 31 years. Figure 8d–f show the difference of 850-hPa wind and SLP between the above three sensitivity

Table 1 Description of control and sensitivity experiments in ECHAM5

Exp. name	SST boundary condition
Control	Climatological SST with seasonal cycle
Run_NIO-WP_0.5	The equal magnitude of 0.5 °C SST anomalies in the NIO (0° S–20° N, 0°–360°) and − 0.5 °C SST anomalies in the WP (− 15° S–15° N, 140° E–180° E) are added on the climatological SST
Run_NIO-WP_1.0	Similar to Run_NIO-WP_0.5, but with the equal magnitude of 1.0 °C
Run_NIO-WP_1.5	Similar to Run_NIO-WP_0.5, but with the equal magnitude of 1.5 °C

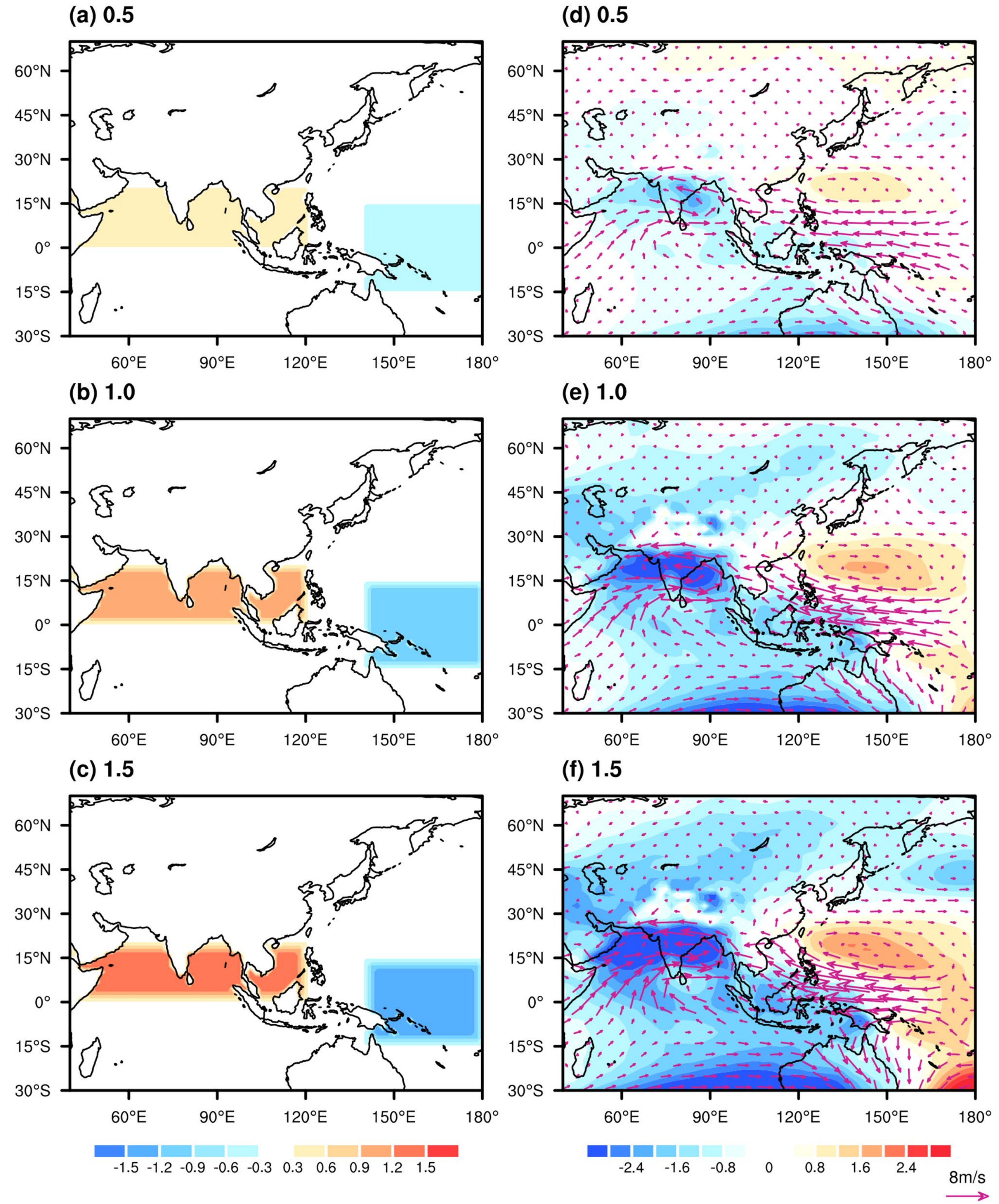

Fig. 8 The anomalies of 850-hPa winds (vectors) and SLP (contours) respond (**d–f**) to the anomalous NIO SST warming and WP SST cooling with the magnitude of 0.5 °C (**a**), 1.0 °C (**b**) and 1.5 °C (**c**), respectively

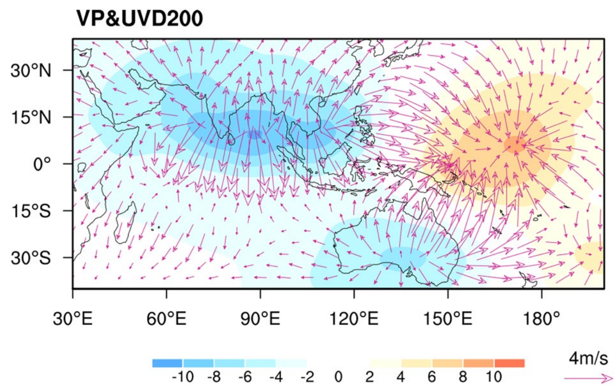

Fig. 9 The anomalies of velocity potential (shading, 10^6 m^2 s^{-1}), and divergence winds at 200 hPa (vectors, ms^{-1}) respond to the anomalous NIO SST warming and WP SST cooling with the magnitude of 1.5 °C

runs and the control run. In response to the east–west contrasting SST anomalies between the NIO and the tropical Pacific, there are significant anticyclonic anomalies over the tropical NWP and the intensity of anticyclonic circulation increase with the increase of the NIO-WP SST gradient.

Figure 9 shows the difference of upper-level potential velocity and divergent winds between the Run_NIO-WP_1.5 experiment and the control run. It can be seen that the east–west SST gradient induces a weakened walker circulation with obvious upper-level divergent anomalies over the NIO and convergence over the western Pacific. Consequently, the atmospheric convection over the tropical west Pacific will be suppressed, which could lead to an anomalous anticyclone in the Northwest Pacific via a Rossby wave response (Wang et al. 2003; Xie et al. 2009, 2016).

6 Summary

This study investigated the role of internal variability on the multidecadal variation of East Asian summertime precipitation trends using three large ensemble simulations that are based on CCSM4, CESM and MPI-ESM. In each of the three large ensembles, although the individual members are forced by the same external forcing and are conducted by the same model, summer rainfall trends in EA–NWP during 1970–2005 show a large diversity across the individual ensemble members. The signal-to-noise ratio between ensemble-mean trend and standard deviation is much smaller than one in most of these regions, suggesting that internally-generated variability is larger than external forcing-induced rainfall changes during the interval in the simulations.

We found that the diversity of summer rainfall trends among the individual members are organized into some coherent patterns in the regions of East Asia and the subtropical NWP. In all the three models, the first leading mode of rainfall trends features a meridional dipole pattern, with drying trends over the subtropical NWP and wetting trends in the Mei-yu Front rainfall belt (20°–35° N). The leading mode is significantly positive correlated with SST over the NIO but negative correlated with SST over the tropical western and central Pacific. The NIO-WP SST gradient could weaken the walker circulation and suppress atmospheric convection over the tropical western Pacific. The suppressed convection could trigger an anomalous anticyclone to the northwest via a Rossby wave response. The anomalous anticyclone will develop over the tropical Northwest Pacific via convective-circulation feedback (Wang et al. 2003; Xie et al. 2009) and extracting kinety energy from mean flow (Hu et al. 2019). Finally, the anomalous anticyclone will suppress Northwest Pacific summer monsoon and enhance East Asian monsoon, leading to the dipole rainfall trends over the EA–NWP. Thus, the meridional dipole pattern rainfall trends over the EA–NWP can result from the internally-generated gradient of NIO-WP SST trends on the multidecadal time scale.

Acknowledgements The study is jointly supported by the National Basic Research Program of China (2019YFA0606703), the Strategic Priority Research Program of Chinese Academy of Sciences (XDA20060502), and the National Natural Science Foundation of China (41425086, 41661144016, 41706026, 41506003, and 41731173). The authors declare no competing interests.

References

Byrne MP, O'Gorman PA (2015) The Response of Precipitation Minus Evapotranspiration to Climate Warming: why the "Wet-Get-Wetter, Dry-Get-Drier" Scaling Does Not Hold over Land*. J Clim 28:8078–8092. https://doi.org/10.1175/jcli-d-15-0369.1

Byrne MP, O'Gorman PA (2013) Link between land-ocean warming contrast and surface relative humidities in simulations with coupled climate models. Geophys Res Lett 40:5223–5227. https://doi.org/10.1002/grl.50971

Cao J, Lu R, Hu J, Wang H (2013) Spring Indian Ocean-western Pacific SST contrast and the East Asian summer rainfall anomaly. Adv Atmos Sci 30:1560–1568. https://doi.org/10.1007/s00376-013-2298-6

Chen W, Park J-K, Dong B, Lu R, Jung W-S (2012) The relationship between El Niño and the western North Pacific summer climate in a coupled GCM: Role of the transition of El Niño decaying phases. J Geophys Res Atmos. https://doi.org/10.1029/2011jd017385

Chou C, Neelin JD (2004) Mechanisms of global warming impacts on regional tropical precipitation. J Clim 17:2688–2701. https://doi.org/10.1175/1520-0442(2004)017%3c2688:Mogwio%3e2.0.Co;2

Chou C, Neelin JD, Chen C-A, Tu J-Y (2009) Evaluating the "rich-get-richer" mechanism in tropical precipitation change under global warming. J Clim 22:1982–2005. https://doi.org/10.1175/2008jcli2471.1

Deser C, Knutti R, Solomon S, Phillips AS (2012a) Communication of the role of natural variability in future North American climate.

Nat Clim Change 2:775–779. https://doi.org/10.1038/nclimate1562
Deser C, Phillips A, Bourdette V, Teng HJCD (2012b) Uncertainty in climate change projections: the role of internal variability. Clim Dyn 38:527–546. https://doi.org/10.1007/s00382-010-0977-x
Ding Y, Wang Z, Sun Y (2008) Inter-decadal variation of the summer precipitation in East China and its association with decreasing Asian summer monsoon. Part I: observed evidences. Int J Climatol 28:1139–1161. https://doi.org/10.1002/joc.1615
Dong B, Sutton RT, Highwood EJ, Wilcox LJ (2015) Preferred response of the East Asian summer monsoon to local and non-local anthropogenic sulphur dioxide emissions. Clim Dyn 46:1733–1751. https://doi.org/10.1007/s00382-015-2671-5
Gent PR et al (2011) The community climate system model version 4. J Clim 24:4973–4991. https://doi.org/10.1175/2011jcli4083.1
Gong D-Y, Ho C-H (2002) Shift in the summer rainfall over the Yangtze River valley in the late 1970s. Geophys Res Lett 29:78-71–78-74. https://doi.org/10.1029/2001gl014523
He C, Zhou T (2015) Decadal change of the connection between summer western North Pacific Subtropical High and tropical SST in the early 1990s. Atmos Sci Lett 16:253–259. https://doi.org/10.1002/asl2.550
He B, Bao Q, Li J, Wu G, Liu Y, Wang X, Sun Z (2012) Influences of external forcing changes on the summer cooling trend over East Asia. Clim Change 117:829–841. https://doi.org/10.1007/s10584-012-0592-4
He C, Zhou T, Li T (2019) Weakened anomalous Western North Pacific anticyclone during an El Niño–decaying summer under a warmer climate: dominant role of the weakened impact of the tropical Indian Ocean on the atmosphere. J Clim 32:213–230. https://doi.org/10.1175/jcli-d-18-0033.1
Held IM, Soden BJ (2006) Robust responses of the hydrological cycle to global warming. J Clim 19:5686–5699. https://doi.org/10.1175/jcli3990.1
Hu Z-Z (1997) Interdecadal variability of summer climate over East Asia and its association with 500 hPa height and global sea surface temperature. J Geophys Res Atmos 102:19403–19412. https://doi.org/10.1029/97jd01052
Hu K, Huang G, Xie S-P (2018) Assessing the internal variability in multi-decadal trends of summer surface air temperature over East Asia with a large ensemble of GCM simulations. Clim Dyn 52:6229–6242. https://doi.org/10.1007/s00382-018-4503-x
Hu K, Huang G, Xie S-P, Long S-M (2019) Effect of the mean flow on the anomalous anticyclone over the Indo-Northwest Pacific in post-El Niño summers. Clim Dyn. https://doi.org/10.1007/s00382-019-04893-z
Huang R, Sun F (1992) Impacts of the Tropical Western Pacific on the East Asian Summer Monsoon. J Meteorol Soc Jpn Ser II 70:243–256. https://doi.org/10.2151/jmsj1965.70.1B_243
Huang R, Wu Y (1989) The influence of ENSO on the summer climate change in China and its mechanism. Adv Atmos Sci 6:21–32. https://doi.org/10.1007/bf02656915
Huang R, Chen J, Huang G (2007) Characteristics and variations of the East Asian monsoon system and its impacts on climate disasters in China. Adv Atmos Sci 24:993–1023. https://doi.org/10.1007/s00376-007-0993-x
Hurrell JW et al (2013) The community earth system model: a framework for collaborative research. Bull Am Meteorol Soc 94:1339–1360. https://doi.org/10.1175/bams-d-12-00121.1
Jiang W, Huang G, Huang P, Wu R, Hu K, Chen W (2019) Northwest Pacific anticyclonic anomalies during Post–El Niño summers determined by the pace of El Niño Decay. J Clim 32:3487–3503. https://doi.org/10.1175/jcli-d-18-0793.1
Kay JE et al (2015) The Community Earth System Model (CESM) large ensemble project: a community resource for studying climate change in the presence of internal climate variability. Bull Am Meteorol Soc 96:1333–1349. https://doi.org/10.1175/bams-d-13-00255.1
Kosaka Y, Xie SP, Lau NC, Vecchi GA (2013) Origin of seasonal predictability for summer climate over the Northwestern Pacific. Proc Natl Acad Sci 110:7574–7579. https://doi.org/10.1073/pnas.1215582110
Li S, Lu J, Huang G, Hu K (2008) Tropical Indian Ocean basin warming and East Asian summer monsoon: a multiple AGCM study. J Clim 21:6080–6088. https://doi.org/10.1175/2008jcli2433.1
Li H, Dai A, Zhou T, Lu J (2010) Responses of East Asian summer monsoon to historical SST and atmospheric forcing during 1950–2000. Clim Dyn 34:501–514. https://doi.org/10.1007/s00382-008-0482-7
Li X, Xie S-P, Gille ST, Yoo C (2015) Atlantic-induced pan-tropical climate change over the past three decades. Nat Clim Change 6:275–279. https://doi.org/10.1038/nclimate2840
Li G et al (2019) Effect of excessive equatorial Pacific cold tongue bias on the El Niño-Northwest Pacific summer monsoon relationship in CMIP5 multi-model ensemble. Clim Dyn 52:6195–6212. https://doi.org/10.1007/s00382-018-4504-9
Ma Z (2007) The interdecadal trend and shift of dry/wet over the central part of North China and their relationship to the Pacific Decadal Oscillation (PDO). Chin Sci Bull 52:2130–2139. https://doi.org/10.1007/s11434-007-0284-z
Maher N et al (2019) The Max Planck Institute grand ensemble: enabling the exploration of climate system variability. J Adv Model Earth Syst 11:2050–2069. https://doi.org/10.1029/2019ms001639
Menon S, Hansen J, Nazarenko L, Luo Y (2002) Climate effects of black carbon aerosols in China and India. Science 297:2250–2253. https://doi.org/10.1126/science.1075159
Nitta T (1987) Convective activities in the Tropical Western Pacific and their impact on the northern hemisphere summer circulation. J Meteorol Soc Jpn Ser II 65:373–390. https://doi.org/10.2151/jmsj1965.65.3_373
North GR, Bell TL, Cahalan RF, Moeng FJ (1982) Sampling errors in the estimation of empirical orthogonal functions. Mon Weather Rev 110:699–706. https://doi.org/10.1175/1520-0493(1982)110%3c0699:Seiteo%3e2.0.Co;2
Ohba M, Ueda H (2006) A role of zonal gradient of SST between the Indian Ocean and the Western Pacific in Localized Convection around the Philippines. Sola 2:176–179. https://doi.org/10.2151/sola.2006-045
Qian C, Zhou T (2014) Multidecadal variability of North China aridity and its relationship to PDO during 1900–2010. J Clim 27:1210–1222. https://doi.org/10.1175/jcli-d-13-00235.1
Roeckner E, Bäuml G, Bonaventura L, Brokopf R, Esch M, Giorgetta (2003) The atmospheric general circulation model ECHAM 5. PART I: model description. MPI Tech Rep. http://hdl.handle.net/11858/00-001M-0000-0012-0144-5
Schiemann R, Lüthi D, Schär C (2009) Seasonality and interannual variability of the westerly jet in the Tibetan Plateau Region. J Clim 22:2940–2957. https://doi.org/10.1175/2008jcli2625.1
Song F, Zhou T (2015) The crucial role of internal variability in modulating the decadal variation of the East Asian Summer Monsoon–ENSO relationship during the twentieth century. J Clim 28:7093–7107. https://doi.org/10.1175/jcli-d-14-00783.1
Song F, Zhou T, Qian Y (2014) Responses of East Asian summer monsoon to natural and anthropogenic forcings in the 17 latest CMIP5 models. Geophys Res Lett 41:596–603. https://doi.org/10.1002/2013gl058705
Takaya K, Nakamura H (2001) A formulation of a phase-independent wave-activity flux for stationary and migratory quasigeostrophic Eddies on a zonally varying basic flow. J Atmos Sci 58:608–627. https://doi.org/10.1175/1520-0469(2001)058%3c0608:Afoapi%3e2.0.Co;2

Terao T (2005) East-west SST contrast over the tropical oceans and the post El Niño western North Pacific summer monsoon. Geophys Res Lett. https://doi.org/10.1029/2005gl023010

Tian F, Dong B, Robson J, Sutton R (2018) Forced decadal changes in the East Asian summer monsoon: the roles of greenhouse gases and anthropogenic aerosols. Clim Dyn 51:3699–3715. https://doi.org/10.1007/s00382-018-4105-7

Ueda H, Kamae Y, Hayasaki M, Kitoh A, Watanabe S, Miki Y, Kumai A (2015) Combined effects of recent Pacific cooling and Indian Ocean warming on the Asian monsoon. Nat Commun 6:8854. https://doi.org/10.1038/ncomms9854

Wallace JM, Fu Q, Smoliak BV, Lin P, Johanson CM (2012) Simulated versus observed patterns of warming over the extratropical Northern Hemisphere continents during the cold season. Proc Natl Acad Sci 109:14337–14342. https://doi.org/10.1073/pnas.1204875109

Wang H (2001) The weakening of the Asian monsoon circulation after the end of 1970's. Adv Atmos Sci 18:376–386. https://doi.org/10.1007/bf02919316

Wang B, Wu R, Li T (2003) Atmosphere-warm ocean interaction and its impacts on Asian-Australian monsoon variation*. J Clim 16(8):1195–1211. https://doi.org/10.1175/1520-0442(2003)16<1195:Aoiaii>2.0.Co;2

Wang B, Ding Q, Jhun J-G (2006) Trends in Seoul (1778–2004) summer precipitation. Geophys Res Lett. https://doi.org/10.1029/2006gl026418

Wang B, Xiang B, Lee JY (2013a) Subtropical high predictability establishes a promising way for monsoon and tropical storm predictions. Proc Natl Acad Sci 110:2718–2722. https://doi.org/10.1073/pnas.1214626110

Wang T, Wang HJ, Otterå OH, Gao YQ, Suo LL, Furevik T, Yu L (2013b) Anthropogenic agent implicated as a prime driver of shift in precipitation in eastern China in the late 1970s. Atmos Chem Phys 13:12433–12450. https://doi.org/10.5194/acp-13-12433-2013

Wang H, Xie X, Liu X (2015) On the robustness of the weakening effect of anthropogenic aerosols on the East Asian summer monsoon with multimodel results. Adv Meteorol 2015:1–8. https://doi.org/10.1155/2015/397395

Wu R, You T, Hu K (2019) What formed the North–South contrasting pattern of summer rainfall changes over Eastern China? Curr Clim Change Rep. https://doi.org/10.1007/s40641-019-00124-z

Xiang B, Wang B, Yu W, Xu S (2013) How can anomalous western North Pacific Subtropical High intensify in late summer? Geophys Res Lett 40:2349–2354. https://doi.org/10.1002/grl.50431

Xie S-P, Hu K, Hafner J, Tokinaga H, Du Y, Huang G, Sampe T (2009) Indian Ocean capacitor effect on Indo-Western Pacific climate during the summer following El Niño. J Clim 22:730–747. https://doi.org/10.1175/2008jcli2544.1

Xie S-P, Kosaka Y, Du Y, Hu K, Chowdary JS, Huang G (2016) Indo-western Pacific ocean capacitor and coherent climate anomalies in post-ENSO summer: a review. Adv Atmos Sci 33:411–432. https://doi.org/10.1007/s00376-015-5192-6

Xu Q (2001) Abrupt change of the mid-summer climate in central east China by the influence of atmospheric pollution. Atmos Environ 35:5029–5040. https://doi.org/10.1016/S1352-2310(01)00315-6

Yang J, Liu Q, Xie S-P, Liu Z, Wu L (2007) Impact of the Indian Ocean SST basin mode on the Asian summer monsoon. Geophys Res Lett. https://doi.org/10.1029/2006gl028571

Yu R, Zhou T (2007) Seasonality and three-dimensional structure of interdecadal change in the East Asian Monsoon. J Clim 20:5344–5355. https://doi.org/10.1175/2007jcli1559.1

Yu R, Wang B, Zhou T (2004) Tropospheric cooling and summer monsoon weakening trend over East Asia. Geophys Res Lett. https://doi.org/10.1029/2004gl021270

Zhang L, Zhou T (2015) Drought over East Asia: a review. J Clim 28:3375–3399. https://doi.org/10.1175/jcli-d-14-00259.1

Zhou T, Gong D, Li J, Li B (2009a) Detecting and understanding the multi-decadal variability of the East Asian Summer Monsoon Recent progress and state of affairs. Meteorol Z 18:455–467. https://doi.org/10.1127/0941-2948/2009/0396

Zhou T et al (2009b) Why the Western Pacific subtropical high has extended westward since the late 1970s. J Clim 22:2199–2215. https://doi.org/10.1175/2008jcli2527.1